European Journal of Pharmaceutics and Biopharmaceutics 137 (2019) 37–45

Contents lists available at ScienceDirect

European Journal of Pharmaceutics and Biopharmaceutics

journal homepage: www.elsevier.com/locate/ejpb

Research paper

Silk fibroin nanoparticles for celecoxib and curcumin delivery: ROS-scavenging and anti-inflammatory activities in an *in vitro* model of osteoarthritis

Barbara Crivelli[a,1], Elia Bari[a,1], Sara Perteghella[a,b,*], Laura Catenacci[a], Milena Sorrenti[a], Michela Mocchi[a,c], Silvio Faragò[d], Giuseppe Tripodo[a], Adriele Prina-Mello[c], Maria Luisa Torre[a,b]

[a] University of Pavia, Department of Drug Sciences, 27100 Pavia, Italy
[b] Pharmaexceed srl, 27100 Pavia, Italy
[c] Trinity College Dublin, The University of Dublin, Laboratory of Biological Characterisation of Advanced Materials, Trinity Translational Medicine Institute, Dublin, Ireland
[d] Silk Division, Innovhub, Stazioni Sperimentali per l'Industria, 20133 Milan, Italy

ARTICLE INFO

Keywords:
Osteoarthritis
Nanoparticles
Drug delivery systems
Silk fibroin
Curcumin
Celecoxib

ABSTRACT

This paper aims at demonstrating silk fibroin nanoparticles (SFNs) promote anti-inflammatory properties of celecoxib (CXB) or curcumin (CUR), and could be exploited for osteoarthritis (OA) treatment. Nanoparticles were prepared by desolvation method and physico-chemically characterized (FT-IR, DSC, TGA, SEM, size distribution and drug release); empty and drug loaded nanoparticles were tested for their ROS-scavenging activity, hemolytic properties, cytotoxicity, and anti-inflammatory potency in an OA *in vitro* model. Results indicate that a controlled drug release has been achieved by varying the drug loading. Curcumin plus SFNs exhibited a synergistic antioxidant effect, while CXB was, in some manner, inhibitory. Both free drugs resulted highly cytotoxic while cell viability reached high values when encapsulated in SFNs. No appreciable differences in anti-inflammatory activity was evidenced between CUR loaded SFNs and CXB. In conclusion, SFNs is an optimal carrier to improve cyto- and hemo-compatibility of both CUR and CXB.

1. Background

Osteoarthritis (OA) represents a pathological condition characterized by both inflammation and chronic degeneration of musculoskeletal compartment, which is triggered by an overproduction of interleukin-1β (IL-1β) and tumour necrosis factor-α (TNF-α), leading to extracellular matrix degradation and cartilage tissue damage. Moreover, cytokine-activated chondrocytes, in inflammatory conditions, over-expressed several cytokines and chemokines including Regulated on Activation, Normal T cell Expressed and Secreted (RANTES) [1].

Currently, a standard regenerative therapy for treating OA does not exist: the available pharmacological strategies are several and aimed to reach and modify different biological targets, albeit the majority is targeted to pain relief. Among these, non-steroidal anti-inflammatory drugs (NSAIDs) and cyclooxigenase-2 (COX-2) selective inhibitors such as celecoxib (CXB), are employed for the treatment of symptomatic pain, inflammation and swelling. More recently, polymeric micelles loaded with CXB have been reported to have also anti-angiogenic activity [2].

Since the established pharmacological therapy covers the entire patient lifespan and is characterized by severe long-term side effects or expensiveness, natural herbal compounds have been recently introduced. Among these, curcumin (CUR), a natural hydrophobic polyphenol extracted from the *Curcuma longa* rhizome, has shown to retain remarkable anti-inflammatory and antioxidant properties exploitable in musculoskeletal pathologies [3,4].

OA is commonly treated with systemic therapies, based on free drugs, albeit they are still suffering from several drawbacks due to their limited solubility [5,6] and consequently poor *in vivo* bioavailability, fast metabolism and bloodstream clearance; these problems could be easily overcome by encapsulating them in nanosystems. Tripodo G, **Perteghella S**, Grisoli P, Trapani A, Torre ML, Mandracchia D (2019). Drug delivery of rifampicin by natural micelles based on inulin: physicochemical properties, antibacterial activity and human macrophages uptake. *European Journal of Pharmaceutics and Biopharmaceutics* **136**: 250-258 doi:10.1016/j.ejpb.2019.01.022. [6–11]. It is therefore to be

* Corresponding author at: Department of Drug Sciences, University of Pavia, Viale Taramelli 12, 27100 Pavia, Italy.
E-mail address: sara.perteghella@unipv.it (S. Perteghella).
[1] These authors contributed equally to this work.

https://doi.org/10.1016/j.ejpb.2019.02.008
Received 19 September 2018; Received in revised form 22 December 2018; Accepted 14 February 2019
Available online 14 February 2019
0939-6411/ © 2019 Elsevier B.V. All rights reserved.

Table 1
Nanoparticles Formulation and Composition details. The drug loading, the process yield and the encapsulation efficiency (as % w/w) are reported as mean values ± standard errors (ES).

Nanoparticle formulation	Process yield (%) (mean ± SE)	Drug concentration in acetone (mg/ml)	Drug loading (% w/w) (mean ± SE)	Encapsulation efficiency (%) (mean ± SE)
SFNs	88.46 ± 7.83	0.0	0.00	0.00
SFNs/CXB-5	82.58 ± 8.39	0.1	5.29 ± 0.31	11.14 ± 5.85
SFNs/CXB-11	71.62 ± 10.69	0.5	11.40 ± 0.76	5.14 ± 1.94
SFNs/CUR-1.5	71.24 ± 10.64	0.8	1.50 ± 0.11	48.86 ± 9.82

noted, nanoparticles have gained much attention in biomedical and biotechnological fields thanks to their capability to efficiently control the drug release and targeting while protecting them from degradation activities and avoiding undesired side effects, when compared to conventional formulations [12,13]. In this context, silk fibroin stand out for its biocompatibility, biodegradability, appropriate mechanical properties and therapeutic retention at the target site [14–18]. Recently, our research group developed a novel drug delivery system by combining silk fibroin nanoparticles (SFNs) loaded with curcumin (SFNs/CUR) and extracellular vesicles secreted by mesenchymal stem cells (MSCs). SFNs/CUR were successfully taken up by MSCs, showing a cytoplasmic localization; notably, the application of a nanotechnological approach avoided CUR cytotoxic events. Furthermore, MSCs were able to release extracellular vesicles entrapping SFNs/CUR, achieving a novel carrier-in-carrier system. Bari E, Perteghella S, Di Silvestre D, Sorlini M, Catenacci L, Sorrenti M, Marrubini G, Rossi R, Tripodo G, Mauri P, Marazzi M, Torre ML (2018). Pilot production of mesenchymal stem/stromal freeze-dried secretome for cell-free regenerative nanomedicine: a validated GMP-compliant process. *Cells* 7, 190; doi:10.3390/cells7110190; Bari E, Perteghella S, Catenacci L, Sorlini M, Croce S, Mantelli M, Avanzini MA, Sorrenti M, Torre ML (2019). Freeze-dried and GMP-compliant pharmaceuticals containing mesenchymal exosomes for acellular MSC immunomodulant therapy. *Nanomedicine* doi:10.2217/nnm-2018-0240 [19,20].

The aim of the present study is to evaluate the anti-oxidant, anti-inflammatory and cytotoxicity profile of nano-encapsulated CXB and CUR in an OA *in vitro* model. First, SFNs, SFNs/CUR and SFNs/CXB were prepared and characterized in terms of physico-chemical properties, particle size and drug release profile; subsequently, they were *in vitro* tested, in comparison with free drugs, on human inflamed articular chondrocytes, evaluating the effect on cell viability and on secretion of inflammatory mediators, such as nitric oxide (NO), IL-6 and RANTES.

2. Materials and methods

2.1. Materials

Sodium carbonate, lithium bromide, acetone, CUR, CXB, ethanol, methanol, collagenase IA, 3-(4,5-dimethylthiazol-2-yl)-2,5-diphenyltetrazolium bromide (MTT) and DMSO were purchased from Sigma-Aldrich (Milan, Italy). Dialysis cellulose tubes were obtained from Visking, Medicell Membranes Ltd (London, UK). 70 μm nylon meshes were obtained from Greiner Bio-One GmbH (Kremsmunster, Austria). Griess Reagent kit was purchased from Biotium (Fremont, California, USA), human RANTES and human IL-6 enzyme-linked immunosorbent assays were obtained from PeproTech (Rocky Hill, USA). All reagents used for cell cultures were purchased from Euroclone (Milan, Italy).

2.2. Silk fibroin extraction

Bombyx mori cocoons were cut and degummed in Na_2CO_3 (0.02 M) aqueous solution for 30 min; degummed fibers were washed in distilled water and dried at room temperature. Silk fibroin (SF) fibers were solubilized in LiBr solution (9.3 M) at 60 °C for 4 h [21,22]; obtained solution was dialyzed against distilled water using dialysis cellulose tubes (3–5 kDa MWCO) at room temperature for 72 h. The SF final concentration, calculated by freeze-drying (Modulyo® Edwards Freeze dryer, Kingston, NY, USA) of known SF volumes, was about 8% w/v.

2.3. Nanoparticles preparation

SF aqueous solution was diluted (1.5% w/v) before carrying out the nanoparticles preparation by desolvation method, as previously reported [19,23]. SF solution was added dropwise to the acetone, leading to the nanoparticles (named SFNs) formation by solvent precipitation. After dialysis (12 kDa MWCO), SFNs suspension were freeze dried at $8*10^{-1}$ mbar and −50° C for long term preservation for further investigations. SFNs loaded with CXB (SFNs/CXB) or with CUR (SFNs/CUR) were obtained dissolving each drug in the respective precipitation solvent (Table 1). Overall, we considered four nanoparticle formulations: SFNs, SFNs/CXB-5, SFNs/CXB-11 (loaded with 5 and 11% w/w of celecoxib, respectively), and SFNs/CUR-1.5 (loaded with 1.5% w/w of curcumin). All formulations were produced in triplicate.

2.4. Characterization of nanoparticles

2.4.1. Drug loading, production yield and encapsulation efficiency evaluation

SFNs drug loading was evaluated by spectrophotometric analysis (Uvikon 860, Kontron Instruments, Zurich, Switzerland) at 254 and 425 nm for CXB and CUR, respectively. Briefly, for each formulation, freeze-dried nanoparticles were dissolved in 96% v/v ethanol (0.1 mg/ml), maintaining mild magnetic stirring in the dark. The total drug content was evaluated from standard calibration curves ($r^2 > 0.9924$ and $r^2 > 0.9902$ for CXB and CUR, respectively), obtained analysing a concentration range of 2.00 – 20.00 μg/ml for CXB, and of 0.25 – 10.00 μg/ml for CUR. Ethanol was considered as blank. Each experiment was performed in triplicate. The drug loading (% w/w) of each formulation was calculated from the ratio between the total drug content (extrapolated from calibration curve) and the concentration of analysed nanoparticles.For each batch, nanoparticle production yield (Y%) was calculated as follow:

$$Y(\%) = \frac{\text{totalweightnanoparticles}}{\text{weightofpolymer} + \text{weightofdrug}} \times 100$$

Encapsulation efficiency (EE%) was determined as percentage ratio between the actual entrapped drug and the drug dissolved in acetone solution during nanoparticle preparation.

2.4.2. Nanoparticles size distribution and evaluation of polydispersity index

The size distribution of nanoparticles was analysed by Nanoparticle Tracking Analysis using NanoSight NS500 equipment (Malvern Instruments, UK). All measurements were repeated for 6 cycles of 60 s each [24].

The polydispersity index (PDI) of each nanoparticle formulation was also determined by Dynamic Light Scattering (DLS Zetasizer Nano S particle analyser, Malvern Instruments). Ten measurements of 300 s each were processed. Samples (0.5 mg/ml aqueous suspension) were sonicated (37 kHz) and filtered (0.45 μm) before carrying out both analyses.

2.4.3. Morphological evaluation by scanning electron microscopy (SEM)

Nanoparticles were observed using SEM (MIRA3, Tescan, Brno, Czech Republic). Briefly, freeze-dried samples were gold-sputter coated under argon prior to perform the morphological analysis measurements.

2.4.4. Fourier transform infrared (FT-IR) spectroscopy

FT-IR spectra of nanoparticles were obtained using a Spectrum One Perkin-Elmer spectrophotometer (Perkin Elmer, Wellesley, MA, USA) equipped with a MIRacle™ ATR device (Pike Technologies, Madison, WI, USA). The IR spectra in transmittance mode where recorded in the spectral region of 650 – 4000 cm^{-1} with a resolution of 4 cm^{-1} [25]. Each experiment was performed in triplicate.

2.4.5. Differential scanning calorimetry (DSC)

Temperature and enthalpy values were measured with a Mettler STARe system (Mettler Toledo, Columbus, OH, USA) equipped with DSC81^e Module and an Intracooler device for sub-ambient temperature analysis (Jukabo FT 900) on about 3 mg of samples in 40 µl sealed aluminium pans with pierced lid (method: −10 – 400 °C temperature range; heating rate 10 K min^{-1}; nitrogen air atmosphere flux 50 ml min^{-1}). The instrument was previously calibrated with Indium, as standard reference. Each experiment was performed in triplicate [26].

2.4.6. Simultaneous thermogravimetric analysis (TGA/DSC 1)

Mass losses were recorded with a Mettler STARe system TGA on 3 – 4 mg samples in 70 µl alumina crucibles with lid (30 – 400 °C temperature range; heating rate 10 K min^{-1}; nitrogen air atmosphere flux 50 ml min^{-1}). The instrument was previously calibrated with Indium, as standard reference and experiments were performed in triplicate.

2.4.7. In vitro drug release

The dialysis technique was applied to investigate the CXB and CUR *in vitro* cumulative release as previously reported, with some modifications [19,27–29]. Briefly, for each batch 15 mg of nanoparticles (SFNs/CXB-5, SFNs/CXB-11 and SFNs/CUR-1.5) were suspended in 4 ml of deionized water and put into dialysis membrane (3 – 5 kDa MWCO). Each dialysis tube was incubated in 10 ml of ethanol/water 50% v/v, maintained under mild magnetic stirring, at 37 °C. At each considered time point, all release medium was removed and replaced with fresh medium to ensure sink conditions. The amount of released drug was determined via spectroscopic method (by reading the release media at 254 and 425 nm for CXB and CUR, respectively). For each considered drug, a calibration curve was prepared (CXB 2.00 – 20.00 µg/ml, r^2 = 0.990; CUR 0.25 – 10.00 µg/ml, r^2 = 0.987). Results were expressed as mean ± standard deviation; for each formulation, three batches were analysed.

2.5. Determination of ROS-scavenging activity by DPPH assay

ROS-scavenging activity of each nanoparticle formulation was evaluated by DPPH assay, according to previous works [30,31]. Briefly, SFNs/CXB-5 and SFNs/CUR-1.5 were tested considering three different nanoparticle concentrations (200, 400 and 800 µg/ml) and their free drug equivalent concentrations calculated from drug loading data (11, 22 and 44 µg/ml for CXB; 3, 6 and 12 µg/ml for CUR) (Table 2).

Samples were resuspended in 70% v/v methanolic solution under magnetic stirring. 50 µl of each considered sample were mixed with 1950 µl of DPPH methanolic solution and incubated, at room temperature, for 60 min avoiding light exposure. Finally, samples were centrifuged (3000 g, 10 min) and the optical density (OD) of supernatants was analyzed at 515 nm. As negative control, a reaction mixture without sample was considered. The percentage of ROS-scavenging activity was calculated according to the following formula:

Table 2
Concentration comparison table for *in vitro* studies (ROS-scavenging, cytoxicity, anti-inflammatory). Drug loading concentrations in SFNs nanoparticles (SFNs/CXB-5 and SFNs/CUR-1.5) compared to the absolute concentrations of free drug (CXB or CUR) calculated by the drug loading data.

	Absolute concentrations of loaded drug (µg/ml) (calculated by the drug loading data)	
Drug loading concentrations into SFNs (µg/ml)	CXB	CUR
200	11	3
400	22	6
800	44	12

$$\text{Antioxidantactivity}(\%) = \frac{(\text{ODctr} - \text{ODsample})}{\text{ODctr}} \times 100$$

where ODctr is the absorbance of negative control and ODsample is that of samples.

2.6. Hemolytic assay

Hemolytic assay was performed on human red blood cells (RBCs), as reported by [32], with some modifications. Human blood samples, collected from three informed healthy donors, were centrifuged at 1500 g for 5 min, to separate RBCs from plasma serum. Obtained RBCs were washed twice with PBS without Ca^{2+} and Mg^{2+} (pH = 7.4). RBCs suspension (90 µl) was co-incubated with freeze-dried nanoparticle suspensions (10 µl) or with free drug (10 µl). For each considered formulation (SFNs/CXB-5 and SFNs/CUR-1.5), nanoparticles were suspended in PBS and sonicated (37 °C, 45 min, 37 kHz) in order to eliminate particle aggregates. For this study, we used three nanoparticle concentrations (200, 400 and 800 µg/ml) and their equivalent free drugs concentration, as reported in Table 2. Untreated RBCs drugs were considered as negative control, while RBCs treated with distilled water as positive control (considered as 100% of hemolysis). After incubation, samples were centrifuged at 3000 g for 10 min. The OD of recovered supernatants were analyzed at 540 nm (Synergy HT, Biotek, Winooski, VT, USA), which corresponds to the absorption maxima of hemoglobin. The overall hemolytic response was evaluated as percentage *versus* controls (Hemolysis%) with the following equation:

$$\text{Hemolysis}(\%) = \frac{(\text{ODsample} - \text{ODnegativeCTR})}{\text{ODpositiveCTR}} \times 100$$

2.7. In vitro biological assays

2.7.1. Human articular chondrocytes isolation and culture

Three knee cartilage samples, obtained during arthroplasty surgery, were cut into 1 – 2 mm^3 segments and washed three times with PBS before being digested with trypsin-EDTA 1X, for 30 min, 37 °C, 5% CO_2, followed by overnight incubation with 200 IU type IA collagenase. The resulting cell suspension was filtered using 70 µm nylon meshes to completely remove undigested tissue and cells were centrifuged at 300 g for 5 min. Obtained chondrocytes were seeded onto flasks (7000 cells/cm^2) with Dulbecco's Modified Eagle's Medium High Glucose (DMEM-HG) enriched in 10% fetal bovine serum (FBS), penicillin (100 IU/ml), streptomycin (100 µg/ml), amphotericin B (2.5 µg/ml), Fibroblast Growth Factor-2 (FGF-2, 10 µg/ml) and Transforming Growth Factor beta-1 (TGF-β1, 10 µg/ml) at 37 °C, 5% CO_2. Each cell line was used up to three culture passages. The study was conducted in accordance with the Declaration of Helsinki, and the protocol was approved by the Ethics Committee of ASST Grande Ospedale Metropolitano Niguarda (Milan, Italy) (Ref. 12.11.2009).

2.7.2. Cell metabolic activity evaluation

Chondrocytes metabolic activity was examined using the MTT assay; cells were seeded in 96-well plate (12000 cells/cm^2) and incubated for 72 h with 100 µl of SFNs, SFNs/CXB-5 and SFNs/CUR-1.5 (at 200, 400 and 800 µg/ml concentrations, respectively), and with 100 µl of free drug, considering the equivalent amounts of CXB and CUR contained in the nanoparticles. After incubation time, all samples were removed and 100 µl of MTT solution (0.5 mg/ml) was added to each well for 3 h. After this time, MTT solution was removed and formazan crystals were solubilized with 100 µl of DMSO. The OD was measured using a microplate reader (Synergy HT) at 570 nm and 670 nm (reference wavelength). Relative cell metabolic activity (%) was calculated as follows: 100 × (ODs/ODc), where ODs represents the mean value of the measured optical density of the tested sample and ODc is the mean value of the measured optical density of untreated cells (control).

2.7.3. Chondrocyte stimulation and treatment

Chondrocytes were seeded in 24-well plates (12000 cells/cm^2) and cultured for 24 h; then, cells were stimulated with IL-1β (10 ng/ml) in FBS deprived medium, as reported by [33,34], to reproduce the mechanisms involved in OA raise, and simultaneously treated with nanoparticle samples (and free drugs) for 72 h. Freeze-dried nanoparticle formulations (SFNs, SFNs/CXB-5 and SFNs/CUR-1.5) were re-suspended in cell culture medium and sonicated at 37 kHz for 1 h before carrying out the incubation, while free drugs were solubilized in DMSO (2 mg/ml) and diluted in cell culture medium, achieving the same drug concentration loaded in each considered nanosystem formulation. For biological tests, SFNs, SFNs/CXB-5, SFNs/CUR-1.5 were considered at three different concentrations (200, 400 and 800 µg/ml). IL-1β stimulated chondrocytes, not treated with nanoparticles were considered as positive control, while untreated chondrocytes as negative control.

Supernatants were collected and stored at −80 °C for further quantification of IL-6 and RANTES, by enzyme-linked immunosorbent assay (ELISA); while nitric oxide (NO) was quantified by Griess method on fresh supernatants.

2.7.4. Determination of nitric oxide (NO), IL-6 and RANTES levels

NO released in cell culture supernatants was detected by using the Griess method, following the manufacturer's instructions. The secretion of IL-6 and RANTES was evaluated using a quantitative ELISA kits, according to manufacturer's instructions. IL-1β stimulated chondrocytes, not treated with nanoparticles were considered as positive control, while untreated chondrocytes as negative control.

2.8. Statistical analysis

Raw data of *in vitro* drug release, antioxidant activity, hemolytic assay, cellular viability and *in vitro* biological assays (NO, IL-6 and RANTES levels) were processed using STATGRAPHICS XVII (Statpoint Technologies, Inc., Warrenton, Virginia, U.S.) and a linear generalized Analysis of Variance model (ANOVA) was used to evaluate the data. The *post-hoc* LSD's test for multiple comparisons was employed to analyze the differences between groups. Unless differently specified, data are expressed as mean ± standard deviation. Statistical significance was set at $p \leq 0.05$.

3. Results and discussion

In this research paper, we compared the biological activity and physicochemical properties of two different drugs encapsulated in silk fibroin-based nanoparticles: CXB, a sulfonamide synthetic compound belonging to the COX-2 selective inhibitors class, which is actually employed as the "first choice" for OA treatment, and CUR, a natural polyphenol extracted from the rhizome of *Curcuma Longa*, characterized by anti-inflammatory and antioxidant activities. Albeit CXB is still considered as the best therapeutic option in treating OA pain, its long-term use in high-dosage could trigger severe cardio-toxicity and renal complications [35]. Conversely, CUR showed the ability to attenuate the inflammatory condition related to OA without significant side-effect [36,37]. Unfortunately, both drugs are characterized by low solubility, which determines a low bioavailability. To the best of our knowledge, nanoencapsulation of CXB in fibroin-based systems has not attempted yet. In literature nanocarrier or nanosystems other than SF were proposed such as liposomes [38], solid lipid nanoparticles [39] and micelles [2].

3.1. Nanoparticle characterization

SFNs, SFNs/CXB and SFNs/CUR formulations were obtained via desolvation method, exploiting the solubility of CXB and CUR in acetone (Table 1).

The process yield (%) in SFNs formation ranged from 71.24 ± 10.64 to 88.46 ± 7.83, for SFNs/CUR-1.5 and SFNs, respectively; while the EE (%) ranged from 5.14 ± 1.93 to 48.86 ± 9.82, for SFNs/CXB-11 and SFNs/CUR-1.5, respectively (Table 1). Our assumption is that all drug was completely internalized in the core of nanoparticles, considering the SFNs/CUR-1.5 particle. Conversely, considering the higher drug loading of SFNs/CXB, we expected that, during the nanoparticle formation, the drug is partially absorbed on the surface of nanosystems. Thus partial loss of absorbed drug is occurring during the dialysis purification, causing a reduction of EE values in SNFs/CXB-5 and SFNs/CXB-11.

All nanoparticle formulations showed a mean diameter of about 110 nm (Fig. 1), characterized by a defined distribution, confirming our previous results [19]. The PDI, measured with Zetasizer, was about 0.15 for all formulations, indicating a narrow size distribution of the nanoparticles. SEM morphological investigation showed a spherical shape and confirmed that the encapsulation of both CXB and CUR does not influence the homogeneous size distribution of nanoparticles (Fig. 1). The particle size distribution and morphology of the obtained nanoparticles (Fig. 1) were in agreement with those reported by other researchers [23,39,40].

Nanoparticle formulation	Size (nm)	Mode	d10	d50	d90
SFNs	118.1 ± 1.0	74.5 ± 2.3	64.2 ± 1.2	88.3 ± 0.6	200.2 ± 9.7
SFNs/CXB 5	112.8 ± 4.2	67.9 ± 2.8	53.1 ± 2.2	75.6 ± 3.9	211.7 ± 12.4
SFNs/CXB 11	114.4 ± 1.5	70.1 ± 2.9	62.7 ± 1.8	77.9 ± 2.8	206.4 ± 8.9
SFNs/CUR 1.5	113.2 ± 1.4	92.2 ± 3.8	71.3 ± 1.7	91.2 ± 0.5	177.3 ± 6.9

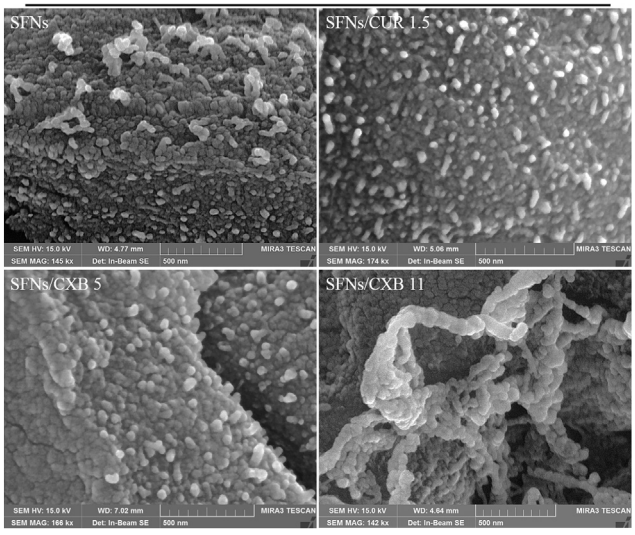

Fig. 1. SEM micrographical images: particle size and morphological investigation of SFNs, SFNs/CXB-5, SFNs/CXB-11 and SFNs/CUR-1.5. NTA results were reported as mean values ± standard deviation.

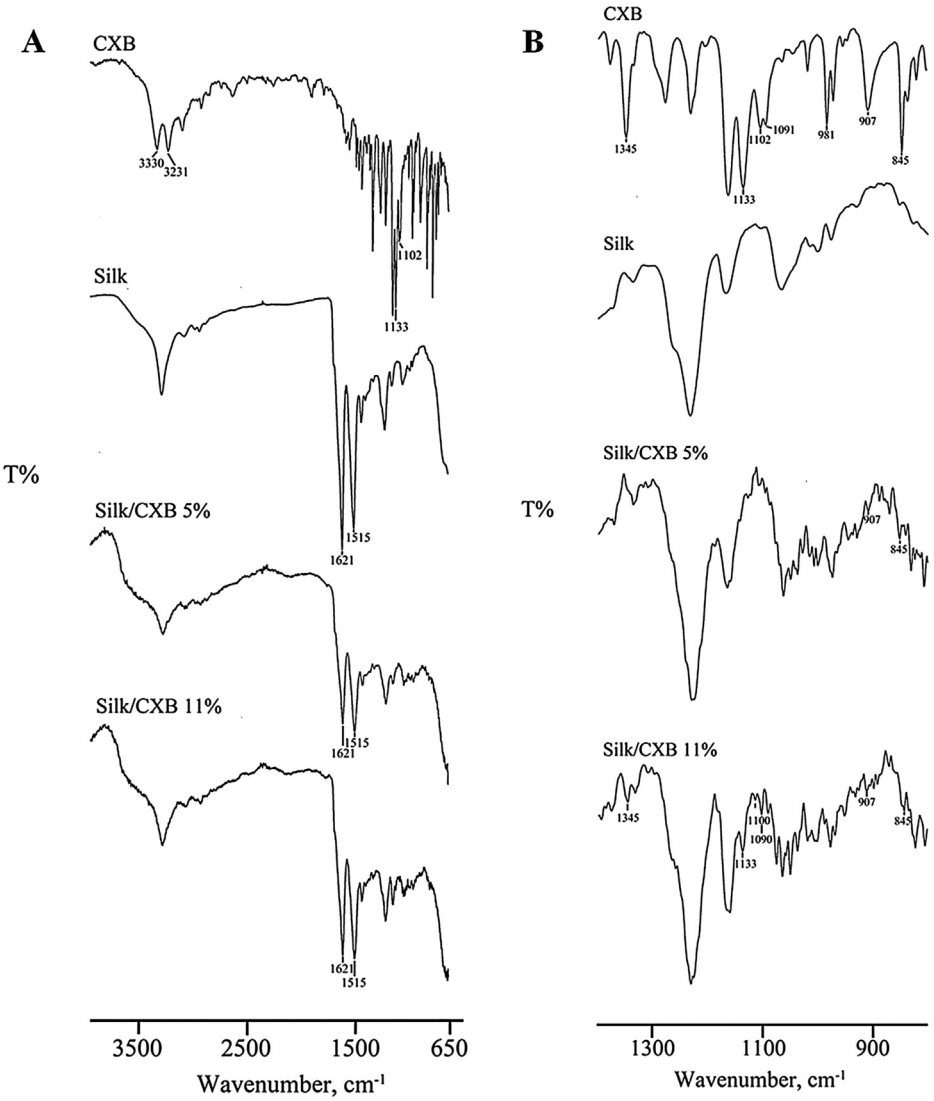

Fig. 2. Fourier transform infrared (FT-IR) spectra of "naked" celcecoxib (CXB), SFNs (silk), SFNs/CXB-5% and SFNs/CXB-11% in the spectral region of 4000 – 650 cm^{-1} (A) and in the region where typical CXB bands appeared (amplified between 1400 and 800 cm^{-1}) (B).

As seen in Table 1, the EE% could appear low in absolute values. These values are under-estimated, due to the absence of specific interactions between the material and the drug (e.g., ionic interactions).

The FT-IR analysis was carried out to confirm the effective nanoencapsulation of the considered active (CXB) into the nanocarrier and to assure the conformational change of SF. In the Fig. 2A are reported the FT-IR spectra of CXB, SFNs, and SFNs/CXB at two different drug concentrations, 5% and 11%, respectively. The IR spectrum of SF showed characteristic peaks that can be identified in the spectra region of amide I (at about 1620 cm^{-1}, C═O stretching), amide II (at about 1520 cm^{-1}, N—H bending) and amide III (at about 1230 cm^{-1}, C—N and N—H functionalities), in all tested formulations (Fig. 2). The FT-IR spectrum of CXB showed the characteristic S═O symmetric and asymmetric stretching in the region 1130 and 1345 cm^{-1}, and the bands of N—H stretching vibration of SO_2NH_2 group at 3330 and 3231 cm^{-1}. The typical absorption bands of CXB are completely hidden for SFNs/CXB-5, while they can be visible in SFNs/CXB-11, related to its higher drug loading. To better compare the spectra of unloaded and loaded nanoparticles, the region between 1500 and 700 cm^{-1} was amplified (Fig. 2B). This has allowed to identify some typical bands of CXB (1345 and 1133 cm^{-1}) only in the spectrum of nanoparticles with higher active content. FT-IR data were supported by thermal analysis. From DSC analysis, CXB results as an anhydrous crystalline compound characterized by melting endothermic peak at 162.6 ± 0.4 °C ($T_{onset,m}$ = 161.1 ± 0.2 °C; ΔH_m = 92.0 ± 1.0 J g^{-1}) with a mass loss recorded in TGA curve (not shown) starting at around 300 °C, due to drug decomposition. The unloaded SFNs showed a typical profile of an amorphous sample with an endothermic effect at around 270 °C, associated to a mass loss in TGA curve, related to sample decomposition. The presence of CXB was also observed in the thermal trace of nanoparticles at the higher drug content, as a small endothermic peak at 161.2 ± 0.6 °C, similarly to the FT-IR spectra. The broad endothermic effects between 30 and 100 °C in the DSC of SFNs/CXB were due to dehydration (mass loss in TGA analyses of about 5.7 ± 0.3%) (not shown).

For SFNs/CUR-1.5 a similar physicochemical characterization was performed and reported in our previous research paper [19]. The FT-IR spectra supported by thermal analysis confirmed also for this system the encapsulation of the drug in SFNs.

3.2. *In vitro drug release studies*

The drug release studies for CXB and CUR showed that both formulation and release-time were statistically significant ($p < 0.0001$) in influencing their performance. Up to three hours, SFNs/CXB-5 and SFNs/CXB-11 formulations showed a similar release profile while, after

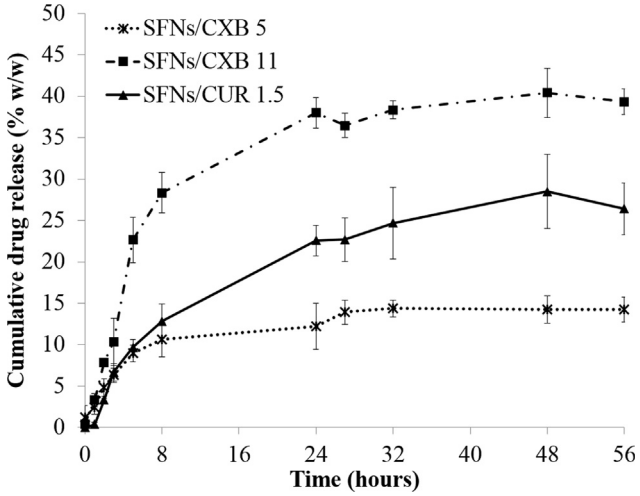

Fig. 3. *In vitro* drug release profiles of SFNs/CXB-5, SFNs/CXB-11 and SFNs/CUR-1.5. Data are reported as cumulative drug release percentage (mean value ± standard deviations) of at least three independent experiments.

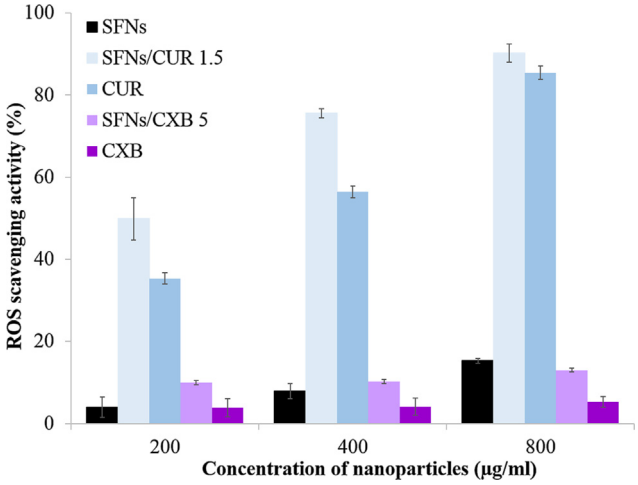

Fig. 4. ROS scavenging activity of SFNs, SFNs/CXB-5, SFNs/CUR-1.5, and equivalent amount of free drugs (CXB and CUR). Data are reported as mean values ± standard deviation of at least three independent experiments.

this time, a different release profile can be seen for the two formulations (Fig. 3). In particular, SFNs/CXB-11 released up to 40% of the whole drug after 24 h; while 14% of CXB was released by SFNs/CXB-5 at the same time. The encapsulation of CXB in fibroin-based nanoparticles improved the drug solubility. Considering the Noyes–Whitney equation, an increase of dissolution rate can be observed when the particle size is reduced. These results were in agreement with other researchers that demonstrated the higher solubility and the increase of release after the encapsulation of CXB in solid-lipid nanoparticles and nanosuspensions [41,42]. The release profiles shown in Fig. 3, suggest that the drug found on the surface or external layer of the nanoparticles is released in a controlled manner up to 8 h for SFNs/CXB-5 and up to 24 h for SFNs/CXB-11. This effect could be simply explained by a controlled dissolution/desorption of the drug from the outer layer of the nanocarrier (SFNs) which makes the nanosystems. This is a fundamental result because allows the preparation of nanosystems with a time-dependent release, controlled by the loaded drug amount.

Considering the release profile of SFNs/CUR-1.5, up to 8 h, a burst release of about 15% was observed (Fig. 3). Silk nanoparticles allowed the drug release of 30%, reaching the plateau after 24 h; these results were in according to our previous research [19] and to the release profile of poor soluble drug loaded in silk nanoparticles [43,44].

3.3. ROS-scavenging activity

Articular chondrocytes degradation is governed by a combination of several mechanisms including an increasing in ROS production, leading to a lack of equilibrium between oxidant and antioxidant systems. For this reason, employing therapeutic molecules with antioxidant properties could ameliorate the symptoms of OA or to prevent structural changes in damaged cartilage [45] with observable clinical benefits.

Thus, here were tested the ROS-scavenging activity of CXB-loaded and CUR-loaded nanoparticles at three concentrations (200, 400 and 800 µg/ml); in particular, for these experiments we selected three nanoparticle formulations (SFNs, SFNs/CXB-5 and SFNs/CUR-1.5) and the equivalent free drugs (CXB and CUR). DPPH assay results showed that formulations and concentrations were statistically significant (ANOVA, $p < 0.0001$); in particular, a dose related response was appreciated for SFNs/CUR 1.5 and free CUR (Fig. 4).

Free CUR exhibits a significant and native antioxidant activity, which becomes higher when included into the SFNs, 80% vs 90% respectively. No statistical differences were observed between SFNs, SFNs/CXB-5 and CXB, since they all showed a ROS scavenging activity lower than 10%. According to other studies, CXB does not show any *in vitro* antioxidant activity [46], while could be slightly increased by SFNs encapsulation (Fig. 4). Based on this finding, we could speculate that the native antioxidant effects of SF and CUR are additive. SFNs resulted as an efficient vehicle for antioxidant compounds, as example curcumin, thanks to the free radical scavenging activity of silk fibroin itself, probably correlated to the aromatic residues present (about 4%) [43,47].

3.4. Hemocompatibility evaluation

Hemocompatibility studies were performed. Considering the hemolytic results (%), ISO/TR 7406 classified the hemolytic effect as: low for values lower than 5, slight for percentages comprised between 5 and 10, and high for values higher than 10. The SFNs were tested at 200 and 400 µg/ml showing a high hemocompatibility, while at 800 µg/ml, our unloaded nanoparticles presented a slight hemolytic effect (Fig. 5). We also tested the hemocompatibility of selected drugs (CXB and CUR), both free and encapsulated in SFNs: our results demonstrated that silk nanoparticles can be considered a good encapsulation method to

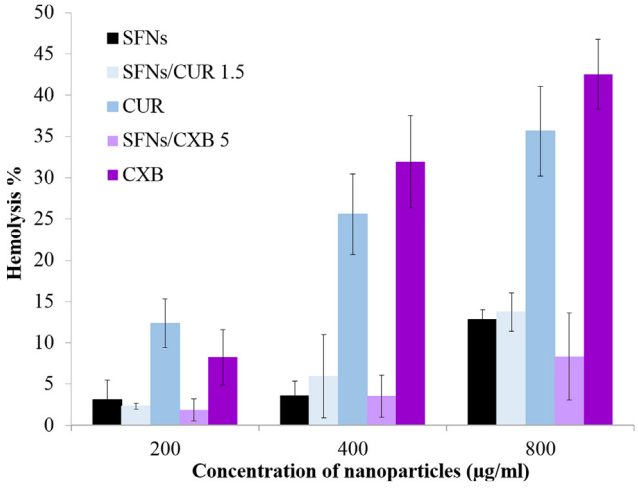

Fig. 5. Hemolysis (%) of Red Blood Cells (RBCs) after treatment with SFNs, SFNs/CUR 1.5, SFNs/CXB 5 (at three different concentrations 200, 400 and 800 µg/ml) and equivalent amount of free drugs (CUR and CXB). Data are reported as mean values ± standard deviation of at least three independent experiments.

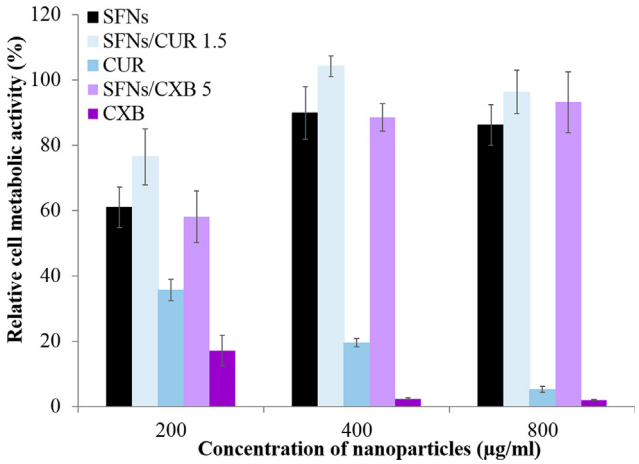

Fig. 6. Relative cell metabolic activity (%) of human articular chondrocytes after treatment (72 h) with SFNs, SFNs/CXB-5 and SFNs/CUR-1.5 (200, 400 and 800 µg/ml) and equivalent amount of free drugs (CXB and CUR). Data are reported as mean values, and relative standard deviations, of at least three independent experiments.

significantly reduce the high hemolytic properties of free CXB and CUR. Free drugs induced a hemolysis percentage higher than 10 already at lower concentration (Fig. 5). Conversely, considering both SFNs/CUR-1.5 and SFNs/CXB-5, we observed a low hemolysis percentage at 200 and 400 µg/ml and a slight hemolysis at 800 µg/ml (Fig. 5).

3.5. Osteoarthritis in vitro model: biological assays

3.5.1. Chondrocyte metabolic activity

To further test the biologic effectiveness of the nanosystems, we tested the effect of free and encapsulated drugs on human articular chondrocytes viability and functionality. Cell metabolic activity was measured by MTT on chondrocytes treated with nanoparticles or with their equivalent free drugs (Table 2) to evaluate their cytotoxicity effect. Both formulations and concentrations were statistically significant (ANOVA, $p < 0.0001$). Drug nanoencapsulation avoided cytotoxicity phenomena, showing viability higher than 70% for all nanoparticle formulations, independently from the employed concentration; on the contrary, free drugs affected cellular viability in a dose dependent manner (Fig. 6).

The encapsulation of CXB and CUR in silk fibroin nanoparticles protected the cells by the cytotoxic effects of free drugs. Chondrocytes maintained a higher cell metabolic activity after treatment with both unloaded and loaded nanoparticles, while free celecoxib and curcumin induced a significant reduction of cell metabolic activity (lower than 40%). In treating OA, cytotoxic events must be avoided because an increase in IL-1β secretion leads to a higher apoptotic events [48]. Previously was reported that the incorporation of CUR into polymeric micelles avoided free drug cytotoxic phenomena, which were observed when employing "naked" CUR [9]. Furthermore, CXB also showed severe cytotoxic effects on several cellular lineages, reaching a viability of 50% at 100 µM concentration [49].

3.5.2. Anti-inflammatory activity of nanoparticles on IL-1β stimulated chondrocytes

We evaluated the cell functionality developing an *in vitro* inflammation model and treating the cells with pro-inflammatory cytokine IL-1β. After the stimulus, we evaluated the secretion of Interleukin-6 (IL-6), a pro-inflammatory cytokine, Nitric Oxide (NO), a compound that promotes chondrocytes apoptosis, and of RANTES, a key mediator of inflammatory condition.

The efficacy of our experimental model was demonstrated by the increase of inflammation mediator release by the cells. The treatment of

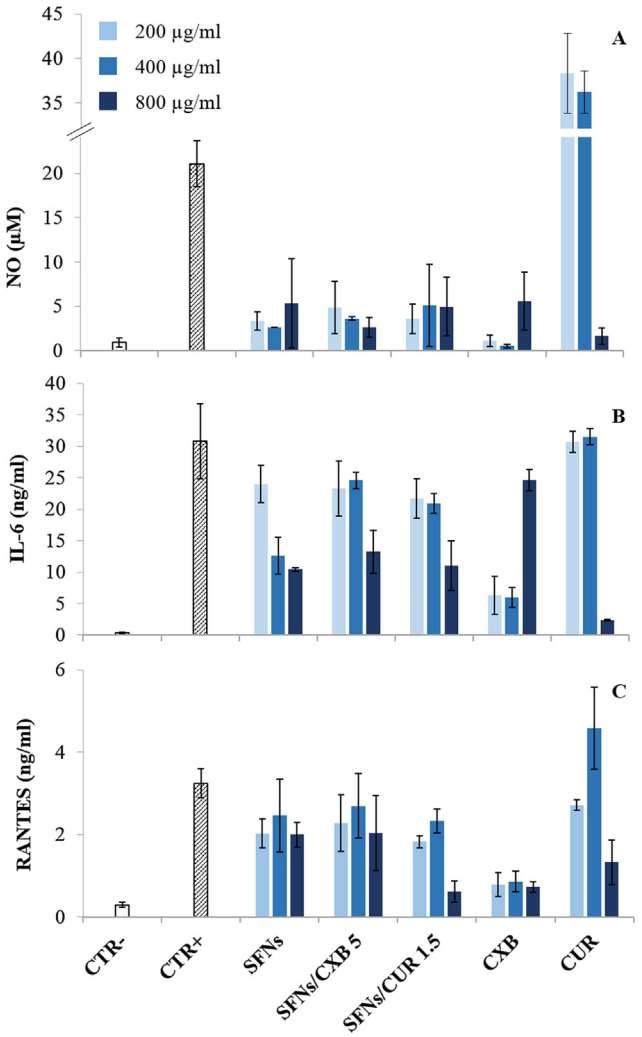

Fig. 7. Production of inflammation mediators NO (A), IL-6 (B) and RANTES (C) by human articular chondrocytes after treatment with pro-inflammatory cytokine IL-1β (10 ng/ml). Cells were stimulated and, at the same time, treated with SFNs, SFNs/CUR-1.5 and SFNs/CXB-5 (200, 400 and 800 µg/ml) and equivalent concentration of free drugs (CUR and CXB). Data are expressed as mean values ± standard deviations (n = 3). Positive control (CTR+) is represented by IL-1β stimulated cells (not treated with samples), while negative control (CTR -) is composed of un-stimulated cells.

chondrocytes with IL-1β (CTR+), compared to untreated cells (CTR -), significant increased ($p < 0.001$) the production of NO (21.09 ± 2.56 and 0.92 ± 0.51 µM, respectively), IL-6 (30.79 ± 5.94 and 0.37 ± 0.13 ng/ml, respectively) and RANTES (3.24 ± 0.354 and 0.29 ± 0.06 ng/ml, respectively).

Considering NO secretion, all nanoparticle formulations, at all considered concentrations, significantly reduced the production of this mediator by the inflamed chondrocytes with respect to positive control (ANOVA, $p < 0.0001$) (Fig. 7A). The inhibition allowed by the nanoparticle treatment was not correlated with the concentration of our nanosystems. Comparing free drugs and positive control, we obtained a significant reduction of NO production ($p < 0.0001$) after the treatment with celecoxib at every investigated concentrations. Conversely, the incubation with lower amounts of curcumin (equivalent to 200 and 400 µg/ml of SFNs/CUR 1.5) induced an increase of inflammation mediator ($p < 0.05$). The NO secretion reduction induced by free CXB could be related to its cytotoxic effect (Fig. 6) that dramatically decreased the cell viability. Here, we hypnotized a low percentage of live cells (low density also) thus not able to secrete a quantifiable amount of

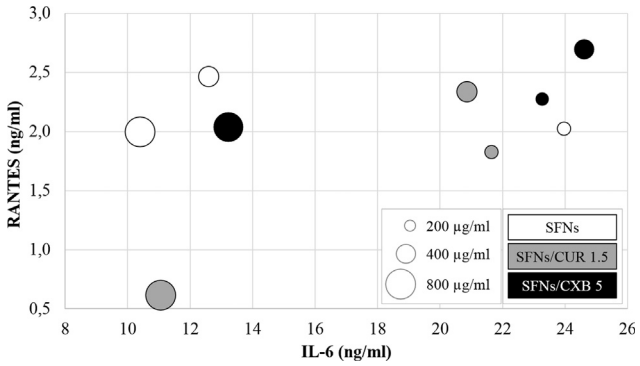

Fig. 8. Relationship between IL-6 and RANTES production by inflamed human chondrocytes after treatment with SFNs (white), SFNs/CUR 1.5 (grey) and SFNs/CXB 5 (black). The diameter of the circles in the plot is proportional to the nanoparticle concentrations: the larger circles correspond to 800 µg/ml, the intermediate circles are those of 400 µg/ml, while smaller circles represent the mediator production after treatment with nanosystems at the concentration 200 µg/ml.

NO. Of interest, SFNs showed the same efficacy in decreasing NO levels with respect to loaded nanoparticles, thus showing an intrinsic anti-inflammatory activity (Fig. 7A).

Concerning the production of IL-6 by stimulated chondrocytes the results show a dose-response for all nanoparticles, with a pronounced effect at higher concentration (800 µg/ml) (ANOVA, $p < 0.0001$) as reported in Fig. 7B. Similarly to NO secretion, the amount of IL-6 significantly decreased when employing SFNs, highlighting its anti-inflammatory potential; in particular the inhibition of IL-6 production was comparably detected with SFNs at 400 µg/ml and the other nanosystems at the highest concentration (800 µg/ml) (Fig. 7B). As obtained for NO, free celecoxib reduced the cell viability and, consequently, the IL-6 secretion. Results obtained after incubation with lower concentrations of free curcumin were no different with respect to positive control, whereas from the higher amount of curcumin we could speculated its cytotoxic effect (Fig. 6) as responsible for the IL-6 level reduction.

Both formulation and concentration were statistically significant for RANTES secretion (ANOVA, $p < 0.0001$); RANTES levels were significantly reduced by all nanoparticle formulations. In particular, SFNs/CUR-1.5, at 800 µg/ml, showed a marked reduction of RANTES (lower than 1 ng/ml) with respect to other considered groups (Fig. 7C). As previously observed, free celecoxib significantly reduced the mediator secretion but could be correlated to its cytotoxic effect. Curcumin resulted as cytotoxic at higher considered concentration while, at lower concentrations induced an increase of RANTES secretion (Fig. 7C).

IL-6 and RANTES dependencies and relationship are reported in Fig. 8. The presence of nanosystems, at the higher concentration (800 µg/ml), decreased both IL-6 and RANTES production. In particular, SFNs/CUR-1.5 showed the most promising results, while SFNs/CXB-5 resulted less efficacious with respect to SFNs at 800 µg/ml.

IL-6 and RANTES expression is regulated by the PKCδ/c-Src/c-Jun and AP-1 signaling pathways, as demonstrated by Tang and colleagues in human synovial fibroblasts [50]. Moreover, CUR is able to reduce iNOS and NO radicals in lipopolysaccharide stimulated rats [51], in both formulation, as free or encapsulated in solid lipid nanoparticles [52].

SF showed an anti-inflammatory activity comparable to that of SFNs/CXB and SFNs/CUR in our *in vitro* model, highlighting its great potential in treating inflammatory diseases. This effect was reported in several biomedical fields: SF peptides, obtained during biodegradation, are the main effectors of anti-inflammatory property [53,54]. SF cannot be considered anymore as an inert polymer, but it must be listed as a "real" active principle ingredient able to effectively inhibit the expression of pro-inflammatory markers, with suitable therapeutic application in inflammatory diseases.

4. Conclusions

This work strongly addresses the use of SFNs as nanodrug delivery systems (DDS) for the treatment of osteoarticular diseases (OA). Advantageously, with a single DDS, we show evidence for a trimodal treatment approach for OA, where to: (i) treating the oxidative stress, (ii) treating the inflammatory pathway and (iii) controlling the drug released over the time.

We demonstrated that, by loading CUR into the SFNs, its intrinsic antioxidant effect is additive to the already one existing by the native SF. Concerning the anti-inflammatory effect, SFNs (unloaded as nanoparticle) and CXB or CUR loaded SFNs (as nanosystem or DDS) showed similar anti-inflammatory magnitude in an *in vitro* model of OA.

These results are fundamental and not trivial since allow to control the time of drug release while maintaining the dose within the expected delivery window. This support the explained biological effects seen over the time and enable the drug release designing from the SFNs by controlling the amount of loaded drug. This is what we demonstrated in this work where at higher drug loadings, corresponds a longer time-release and not a higher dose-release. This opens opportunity for personalised medicine in Osteoarthritis where to fine tune the drug delivery within the effective therapeutic window.

Acknowledgements

This research was partially supported by Artefil S.r.l. (Luisago, CO, Italy), PhD Grant 2017-2019. Authors thank Nembri Industrie Tessili S.r.l. (Capriolo (BG), Italy) for certified Bombyx mori cocoons, Prof. Sergio Schinelli and Dott. Mayra Paolillo (Drug Sciences Dept., Pavia University, Italy) for willingness on the use of Synergy HT (BioTek). A. P.-M. would like to thank Science Foundation Ireland under the Amber Centre Programme for the financial support.

Conflict of interest

S.P. and M.L.T. are members of the advisory board of the company PharmaExceed S.r.l.

Author contributions

Conceptualization and Supervision, M.L.T., S.F. and A.P-M.; Methodology, S.P., M.S., L.C., and G.T.; Investigation, B.C., E.B., S.P., L.C., M.S. and M.M.; Writing-Original Draft Preparation, B.C. and S.P.; Writing-Review & Editing, S.P., G.T., M.S; Final revision A.P.-M., S.P. and M.L.T.

References

[1] N. Alaaeddine, T. Olee, S. Hashimoto, L. Creighton-Achermann, M. Lotz, Production of the chemokine RANTES by articular chondrocytes and role in cartilage degradation, Arthritis Rheum. 44 (2001) 1633–1643.
[2] D. Mandracchia, G. Tripodo, A. Trapani, S. Ruggieri, T. Annese, T. Chlapanidas, G. Trapani, D. Ribatti, Inulin based micelles loaded with curcumin or celecoxib with effective anti-angiogenic activity, Eur. J. Pharm. Sci. 93 (2016) 141–146.
[3] B.B. Aggarwal, K.B. Harikumar, Potential therapeutic effects of curcumin, the anti-inflammatory agent, against neurodegenerative, cardiovascular, pulmonary, metabolic, autoimmune and neoplastic diseases, Int. J. Biochem. Cell Biol. 41 (2009) 40–59.
[4] O. Naksuriya, S. Okonogi, R.M. Schiffelers, W.E. Hennink, Curcumin nanoformulations: a review of pharmaceutical properties and preclinical studies and clinical data related to cancer treatment, Biomaterials 35 (2014) 3365–3383.
[5] S.K. Paulson, M.B. Vaughn, S.M. Jessen, Y. Lawal, C.J. Gresk, B. Yan, T.J. Maziasz, C.S. Cook, A. Karim, Pharmacokinetics of celecoxib after oral administration in dogs and humans: effect of food and site of absorption, J. Pharmacol. Exp. Ther. 297 (2001) 638–645.
[6] L. Catenacci, D. Mandracchia, M. Sorrenti, L. Colombo, M. Serra, G. Tripodo, In-solution structural considerations by H-1 NMR and solid-state thermal properties of inulin-D-alpha-tocopherol succinate (INVITE) micelles as drug delivery systems for

hydrophobic drugs, Macromol. Chem. Phys. 215 (2014) 2084–2096.
[7] S. Onoue, S. Yamada, H.-K. Chan, Nanodrugs: pharmacokinetics and safety, Int. J. Nanomed. 9 (2014) 1025–1037.
[8] G. Tripodo, G. Pasut, A. Trapani, A. Mero, F.M. Lasorsa, T. Chlapanidas, G. Trapani, D. Mandracchia, Inulin-D-alpha-tocopherol succinate (INVITE) nanomicelles as a platform for effective intravenous administration of curcumin, Biomacromolecules 16 (2015) 550–557.
[9] G. Tripodo, T. Chlapanidas, S. Perteghella, B. Vigani, D. Mandracchia, A. Trapani, M. Galuzzi, M.C. Tosca, B. Antonioli, P. Gaetani, M. Marazzi, M.L. Torre, Mesenchymal stromal cells loading curcumin-INVITE-micelles: A drug delivery system for neurodegenerative diseases, Coll. Surf. B-Biointerf. 125 (2015) 300–308.
[10] D. Mandracchia, G. Tripodo, A. Latrofa, R. Dorati, Amphiphilic inulin-d-alpha-tocopherol succinate (INVITE) bioconjugates for biomedical applications, Carbohydr. Polym. 103 (2014) 46–54.
[11] B. Crivelli, S. Perteghella, E. Bari, M. Sorrenti, G. Tripodo, T. Chlapanidas, M.L. Torre, Silk nanoparticles: from inert supports to bioactive natural carriers for drug delivery, Soft Matter 14 (2018) 546–557.
[12] K. Roy, R.K. Kanwar, J.R. Kanwar, Molecular targets in arthritis and recent trends in nanotherapy, Int. J. Nanomed. 10 (2015) 5407–5420.
[13] E. Nogueira, A. Gomes, A. Preto, A. Cavaco-Paulo, Update on therapeutic approaches for rheumatoid arthritis, Curr. Med. Chem. 23 (2016) 2190–2203.
[14] D. Yao, H. Liu, Y. Fan, Silk scaffolds for musculoskeletal tissue engineering, Exp. Biol. Med. 241 (2016) 238–245.
[15] S. Perteghella, B. Vigani, L. Mastracci, F. Grillo, B. Antonioli, M. Galuzzi, M.C. Tosca, B. Crivelli, S. Preda, G. Tripodo, M. Marazzi, T. Chlapanidas, M.L. Torre, Stromal vascular fraction loaded silk fibroin mats effectively support the survival of diabetic mice after pancreatic islet transplantation, Macromol. Biosci. 17 (2017) 1700131.
[16] S. Farago, G. Lucconi, S. Perteghella, B. Vigani, G. Tripodo, M. Sorrenti, L. Catenacci, A. Boschi, M. Faustini, D. Vigo, T. Chlapanidas, M. Marazzi, M.L. Torre, A dry powder formulation from silk fibroin microspheres as a topical auto-gelling device, Pharm. Dev. Technol. 21 (2016) 453–462.
[17] B. Kundu, R. Rajkhowa, S.C. Kundu, X. Wang, Silk fibroin biomaterials for tissue regenerations, Adv. Drug Deliv. Rev. 65 (2013) 457–470.
[18] B. Vigani, L. Mastracci, F. Grillo, S. Perteghella, S. Preda, B. Crivelli, B. Antonioli, M. Galuzzi, M.C. Tosca, M. Marazzi, M.L. Torre, T. Chlapanidas, Local biological effects of adipose stromal vascular fraction delivery systems after subcutaneous implantation in a murine model, J. Bioactive Compatible Polym 31 (2016) 600–612.
[19] S. Perteghella, B. Crivelli, L. Catenacci, M. Sorrenti, G. Bruni, V. Necchi, B. Vigani, M. Sorlini, M.L. Torre, T. Chlapanidas, Stem cell-extracellular vesicles as drug delivery systems: new frontiers for silk/curcumin nanoparticles, Int. J. Pharm. 520 (2017) 86–97.
[20] B. Crivelli, T. Chlapanidas, S. Perteghella, E. Lucarelli, L. Pascucci, A.T. Brini, I. Ferrero, M. Marazzi, A. Pessina, M.L. Torre, Italian mesenchymal stem cell, mesenchymal stem/stromal cell extracellular vesicles: from active principle to next generation drug delivery system, J. Control. Release 262 (2017) 104–117.
[21] D.N. Rockwood, R.C. Preda, T. Yucel, X. Wang, M.L. Lovett, D.L. Kaplan, Materials fabrication from Bombyx mori silk fibroin, Nat. Protoc. 6 (2011) 1612–1631.
[22] D.M. Phillips, L.F. Drummy, D.G. Conrady, D.M. Fox, R.R. Naik, M.O. Stone, P.C. Trulove, H.C. De Long, R.A. Mantz, Dissolution and regeneration of bombyx mori silk fibroin using ionic liquids, J. Am. Chem. Soc. 126 (2004) 14350–14351.
[23] F.P. Seib, G.T. Jones, J. Rnjak-Kovacina, Y. Lin, D.L. Kaplan, pH-Dependent anticancer drug release from silk nanoparticles, Adv. Healthcare Mater. 2 (2013) 1606–1611.
[24] C.M. Maguire, K. Sillence, M. Roesslein, C. Hannell, G. Suarez, J.J. Sauvain, S. Capracotta, S. Contal, S. Cambier, N. El Yamani, M. Dusinska, A. Dybowska, A. Vennemann, L. Cooke, A. Haase, A. Luch, M. Wiemann, A. Gutleb, R. Korenstein, M. Riediker, P. Wick, P. Hole, A. Prina-Mello, Benchmark of nanoparticle tracking analysis on measuring nanoparticle sizing and concentration, J. Micro Nano-Manuf. 5 (2017).
[25] P. Bhatt, R. Lalani, I. Vhora, S. Patil, J. Amrutiya, A. Misra, R. Mashru, Liposomes encapsulating native and cyclodextrin enclosed paclitaxel: Enhanced loading efficiency and its pharmacokinetic evaluation, Int. J. Pharm. 536 (2018) 95–107.
[26] J. Patel, J. Amrutiya, P. Bhatt, A. Javia, M. Jain, A. Misra, Targeted delivery of monoclonal antibody conjugated docetaxel loaded PLGA nanoparticles into EGFR overexpressed lung tumour cells, J. Microencapsul. 35 (2018) 204–217.
[27] J. Shaikh, D.D. Ankola, V. Beniwal, D. Singh, M.N.V.R. Kumar, Nanoparticle encapsulation improves oral bioavailability of curcumin by at least 9-fold when compared to curcumin administered with piperine as absorption enhancer, Eur. J. Pharm. Sci. 37 (2009) 223–230.
[28] D. Mandracchia, A. Trapani, S. Perteghella, M. Sorrenti, L. Catenacci, M.L. Torre, G. Trapani, G. Tripodo, pH-sensitive inulin-based nanomicelles for intestinal site-specific and controlled release of celecoxib, Carbohydr. Polym. 181 (2018) 570–578.
[29] C. Yewale, D. Baradia, S. Patil, P. Bhatt, J. Amrutiya, R. Gandhi, G. Kore, A. Misra, Docetaxel loaded immunonanoparticles delivery in EGFR overexpressed breast carcinoma cells, J. Drug Delivery Sci. Technol. 45 (2018) 334–345.
[30] E. Bari, C.R. Arciola, B. Vigani, B. Crivelli, P. Moro, G. Marrubini, M. Sorrenti, L. Catenacci, G. Bruni, T. Chlapanidas, E. Lucarelli, S. Perteghella, M.L. Torre, In Vitro effectiveness of microspheres based on silk sericin and chlorella vulgaris or arthrospira platensis for wound healing applications, Materials 10 (2017).
[31] T. Chlapanidas, S. Farago, G. Lucconi, S. Perteghella, M. Galuzzi, M. Mantelli, M.A. Avanzini, M.C. Tosca, M. Marazzi, D. Vigo, M.L. Torre, M. Faustini, Sericins exhibit ROS-scavenging, anti-tyrosinase, anti-elastase, and in vitro immunomodulatory activities, Int. J. Biol. Macromol. 58 (2013) 47–56.
[32] S. Maji, I.K. Yan, M. Parasramka, S. Mohankumar, A. Matsuda, T. Patel, In vitro toxicology studies of extracellular vesicles, J. Appl. Toxicol. 37 (2017) 310–318.
[33] M. Galuzzi, S. Perteghella, B. Antonioli, M.C. Tosca, E. Bari, G. Tripodo, M. Sorrenti, L. Catenacci, L. Mastracci, F. Grillo, M. Marazzi, M.L. Torre, Human engineered cartilage and decellularized matrix as an alternative to animal osteoarthritis model, Polymers 10 (2018).
[34] C. Cannava, S. Tommasini, R. Stancanelli, V. Cardile, F. Cilurzo, I. Giannone, G. Puglisi, C.A. Ventura, Celecoxib-loaded PLGA/cyclodextrin microspheres: characterization and evaluation of anti-inflammatory activity on human chondrocyte cultures, Coll. Surf. B-Biointerf. 111 (2013) 289–296.
[35] L.J. Marnett, The COXIB Experience: a look in the rearview mirror, Annu. Rev. Pharmacol. Toxicol. 49 (2009) 265–290.
[36] D.-O. Moon, M.-O. Kim, Y.H. Choi, Y.-M. Park, G.-Y. Kim, Curcumin attenuates inflammatory response in IL-1 beta-induced human synovial fibroblasts and collagen-induced arthritis in mouse model, Int. Immunopharmacol. 10 (2010) 605–610.
[37] Z. Zhang, D.J. Leong, L. Xu, Z. He, A. Wang, M. Navati, S.J. Kim, D.M. Hirsh, J.A. Hardin, N.J. Cobelli, J.M. Friedman, H.B. Sun, Curcumin slows osteoarthritis progression and relieves osteoarthritis-associated pain symptoms in a post-traumatic osteoarthritis mouse model, Arthritis Res. Therapy 18 (2016).
[38] E. Moghimipour, S. Handali, Utilization of thin film method for preparation of celecoxib loaded liposomes, Adv. Pharm. Bull 2 (2012) 93–98.
[39] S. Sharma, S. Bano, A.S. Ghosh, M. Mandal, H.-W. Kim, T. Dey, S.C. Kundu, Silk fibroin nanoparticles support in vitro sustained antibiotic release and osteogenesis on titanium surface, Nanomed.-Nanotechnol. Biol. Med. 12 (2016) 1193–1204.
[40] Y.-Q. Zhang, W.-D. Shen, R.-L. Xiang, L.-J. Zhuge, W.-J. Gao, W.-B. Wang, Formation of silk fibroin nanoparticles in water-miscible organic solvent and their characterization, J. Nanopart. Res. 9 (2007) 885–900.
[41] E.S. Ha, G.H. Choo, I.H. Baek, M.S. Kim, Formulation, characterization, and in vivo evaluation of celecoxib-PVP solid dispersion nanoparticles using supercritical antisolvent process, Molecules 19 (2014) 20325–20339.
[42] S.B. Murdande, D.A. Shah, R.H. Dave, Impact of nanosizing on solubility and dissolution rate of poorly soluble pharmaceuticals, J. Pharm. Sci. 104 (2015) 2094–2102.
[43] M.G. Montalban, J.M. Coburn, A.A. Lozano-Perez, J.L. Cenis, G. Villora, D.L. Kaplan, Production of curcumin-loaded silk fibroin nanoparticles for cancer therapy, Nanomaterials 8 (2018).
[44] P.Y. Wu, Q. Liu, R.T. Li, J. Wang, X. Zhen, G.F. Yue, H.Y. Wang, F.B. Cui, F.L. Wu, M. Yang, X.P. Qian, L.X. Yu, X.Q. Jiang, B.R. Liu, Facile preparation of paclitaxel loaded silk fibroin nanoparticles for enhanced antitumor efficacy by locoregional drug delivery, ACS Appl. Mater. Interf. 5 (2013) 12638–12645.
[45] S.B. Abramson, Nitric oxide in inflammation and pain associated with osteoarthritis, Arthritis Research & Therapy 10 (2008).
[46] S. Sozer, G. Diniz, F. Lermioglu, Effects of celecoxib in young rats: histopathological changes in tissues and alterations of oxidative stress/antioxidant defense system, Arch. Pharmacal Res. 34 (2011) 253–259.
[47] A.A. Lozano-Perez, H.C. Rivero, M.D.P. Hernandez, A. Pagan, M.G. Montalban, G. Villora, J.L. Cenis, Silk fibroin nanoparticles: efficient vehicles for the natural antioxidant quercetin, Int. J. Pharm. 518 (2017) 11–19.
[48] F. Heraud, A. Heraud, M.F. Harmand, Apoptosis in normal and osteoarthritic human articular cartilage, Ann. Rheum. Dis. 59 (2000) 959–965.
[49] M.A. Hashemipour, H. Mehrabizadeh Honarmand, F. Falsafi, M. Tahmasebi Arashlo, S. Rajabalian, S.A.H. Gandjalikhan Nassab, In vitro cytotoxic effects of celecoxib, mefenamic acid, aspirin and indometacin on several cells lines, J. Dentistry (Shiraz, Iran) 17 (2016) 219–225.
[50] C.-H. Tang, C.-J. Hsu, Y.-C. Fong, The CCL5/CCR5 axis promotes interleukin-6 production in human synovial fibroblasts, Arthritis Rheum. 62 (2010) 3615–3624.
[51] M. Onoda, H. Inano, Effect of curcumin on the production of nitric oxide by cultured rat mammary gland, Nitric Oxide-Biol. Chem. 4 (2000) 505–515.
[52] R. Arora, A. Kuhad, I.P. Kaur, K. Chopra, Curcumin loaded solid lipid nanoparticles ameliorate adjuvant-induced arthritis in rats, Eur. J. Pain 19 (2015) 940–952.
[53] A. Rodriguez-Nogales, F. Algieri, L. De Matteis, A. Abel Lozano-Perez, J. Garrido-Mesa, T. Vezza, J.M. de la Fuente, J. Luis Cenis, J. Galvez, M. Elena, Rodriguez-Cabezas, Intestinal anti-inflammatory effects of RGD-functionalized silk fibroin nanoparticles in trinitrobenzenesulfonic acid-induced experimental colitis in rats, Int. J. Nanomed. 11 (2016) 5945–5958.
[54] D.W. Kim, H.S. Hwang, D.-S. Kim, S.H. Sheen, D.H. Heo, G. Hwang, S.H. Kang, H. Kweon, Y.-Y. Jo, S.W. Kang, K.-G. Lee, K.W. Park, K.H. Han, J. Park, W.S. Eum, Y.-J. Cho, H.C. Choi, S.Y. Choi, Effect of silk fibroin peptide derived from silkworm Bombyx mori on the anti-inflammatory effect of Tat-SOD in a mice edema model, Bmb Reports 44 (2011) 787–792.